Supporting Information for

Structural Characterization of Manganese and Iron Complexes with Methylated Derivatives of Bis(2-pyridylmethyl)-1,2-ethanediamine Reveals Unanticipated Conformational Flexibility

Cristina M. Coates, Kenton Hagan, Casey A. Mitchell, John D. Gorden, and Christian R. Goldsmith*

Department of Chemistry & Biochemistry, Auburn University, Auburn, AL 36849

*To whom correspondence should be addressed: crgoldsmith@auburn.edu

Contents

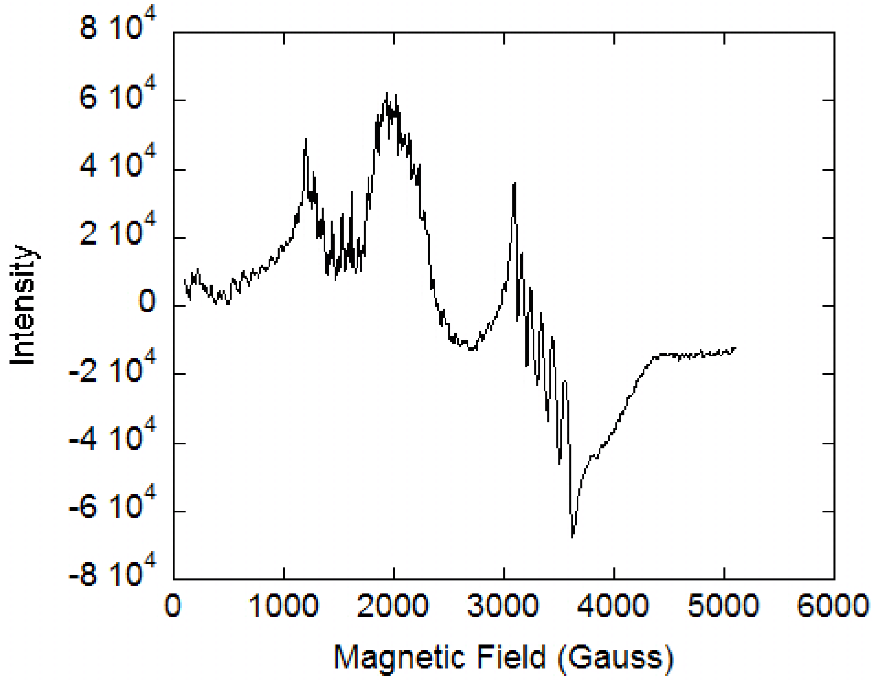

Figure S1. X-band EPR spectrum of a 1 mM sample of [Mn(L)Cl_2] in DMF at 50 K.

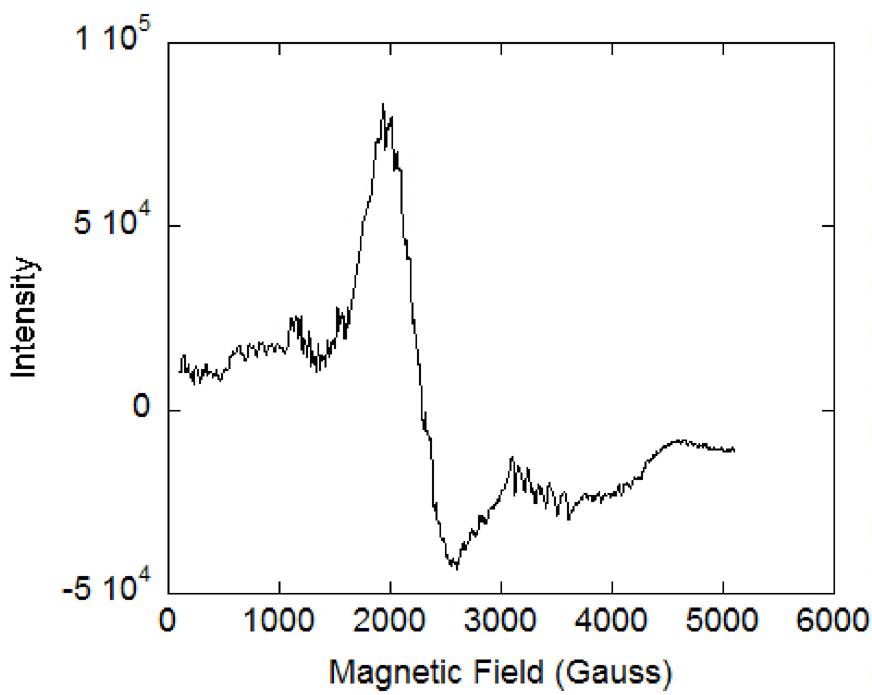

Figure S2. X-band EPR spectrum of a 1 mM sample of [Mn(L^{Me}1)Cl_2] in DMF at 50 K.

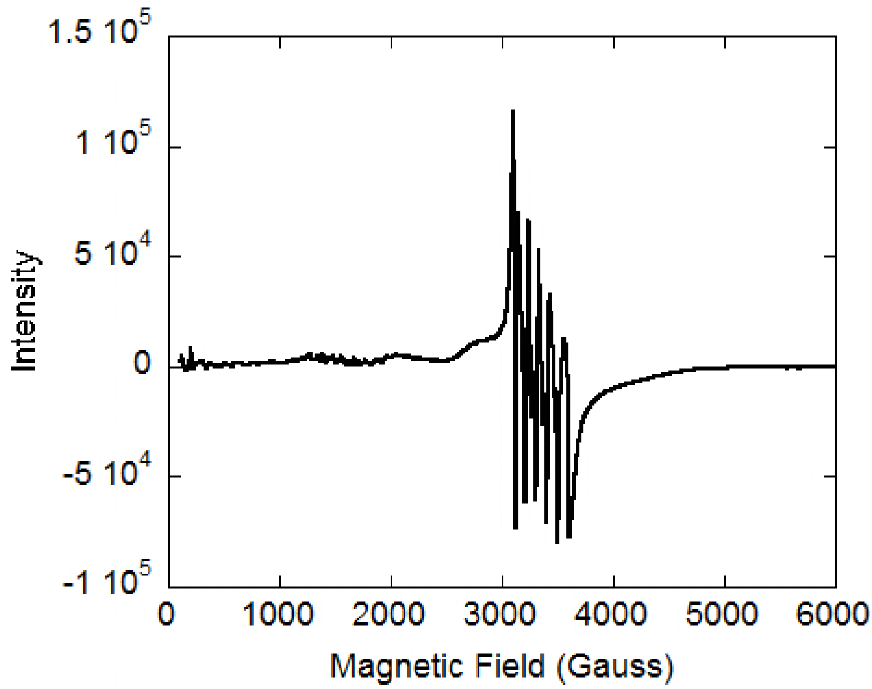

Figure S3. X-band EPR spectrum of a 1 mM sample of $[Mn(L^{Me}2)Cl_2]$ in DMF at 50 K.

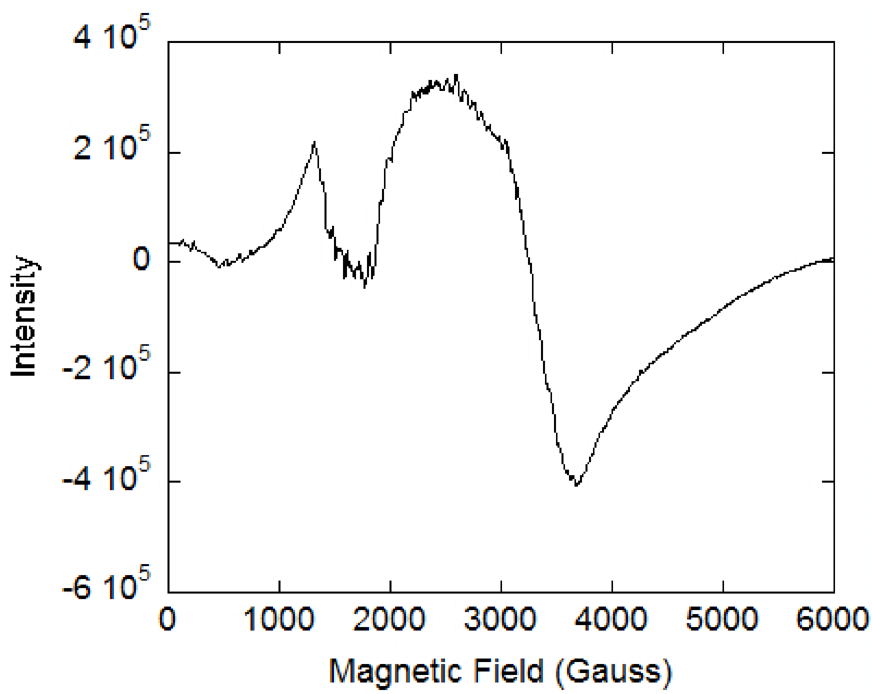

Figure S4. X-band EPR spectrum of a 1 mM sample of $[Mn(L^{Me}2')Cl_2]$ in DMF at 50 K.

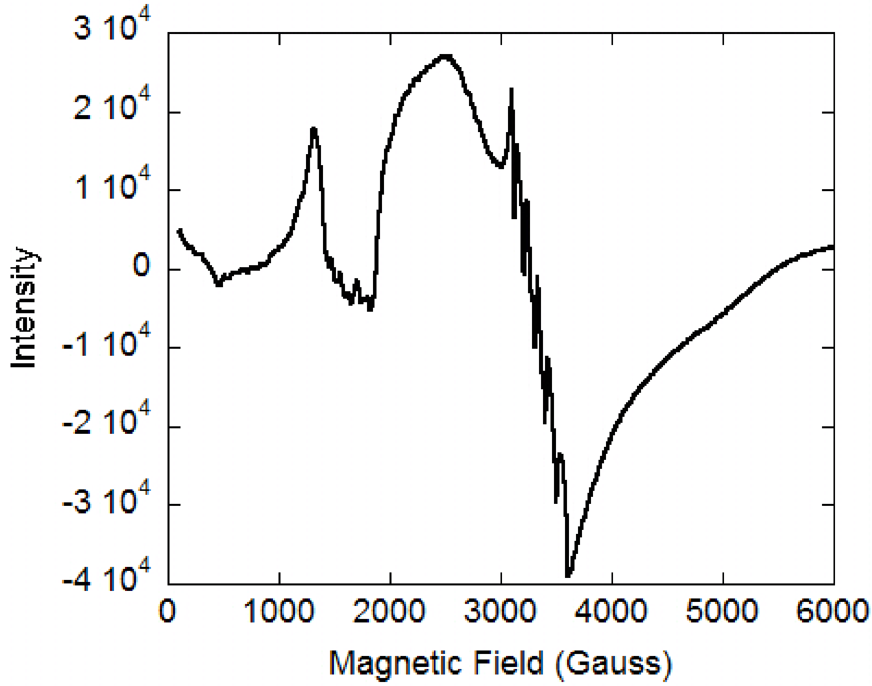

Figure S5. X-band EPR spectrum of a 1 mM sample of [Mn(L^{Me}3)Cl_2] in DMF at 50 K.

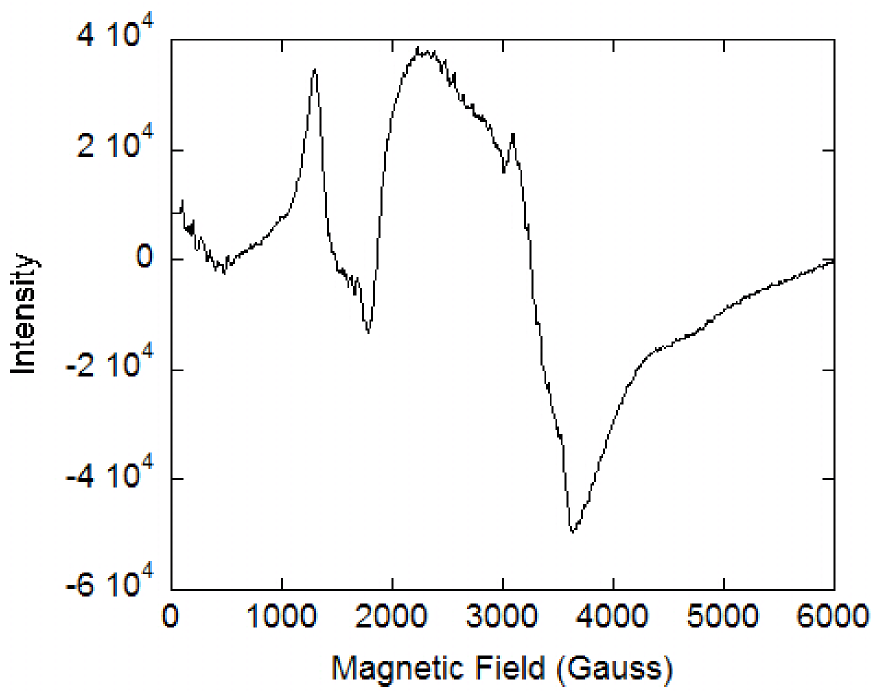

Figure S6. X-band EPR spectrum of a 1 mM sample of [Mn(L^{Me}4)Cl_2] in DMF at 50 K.

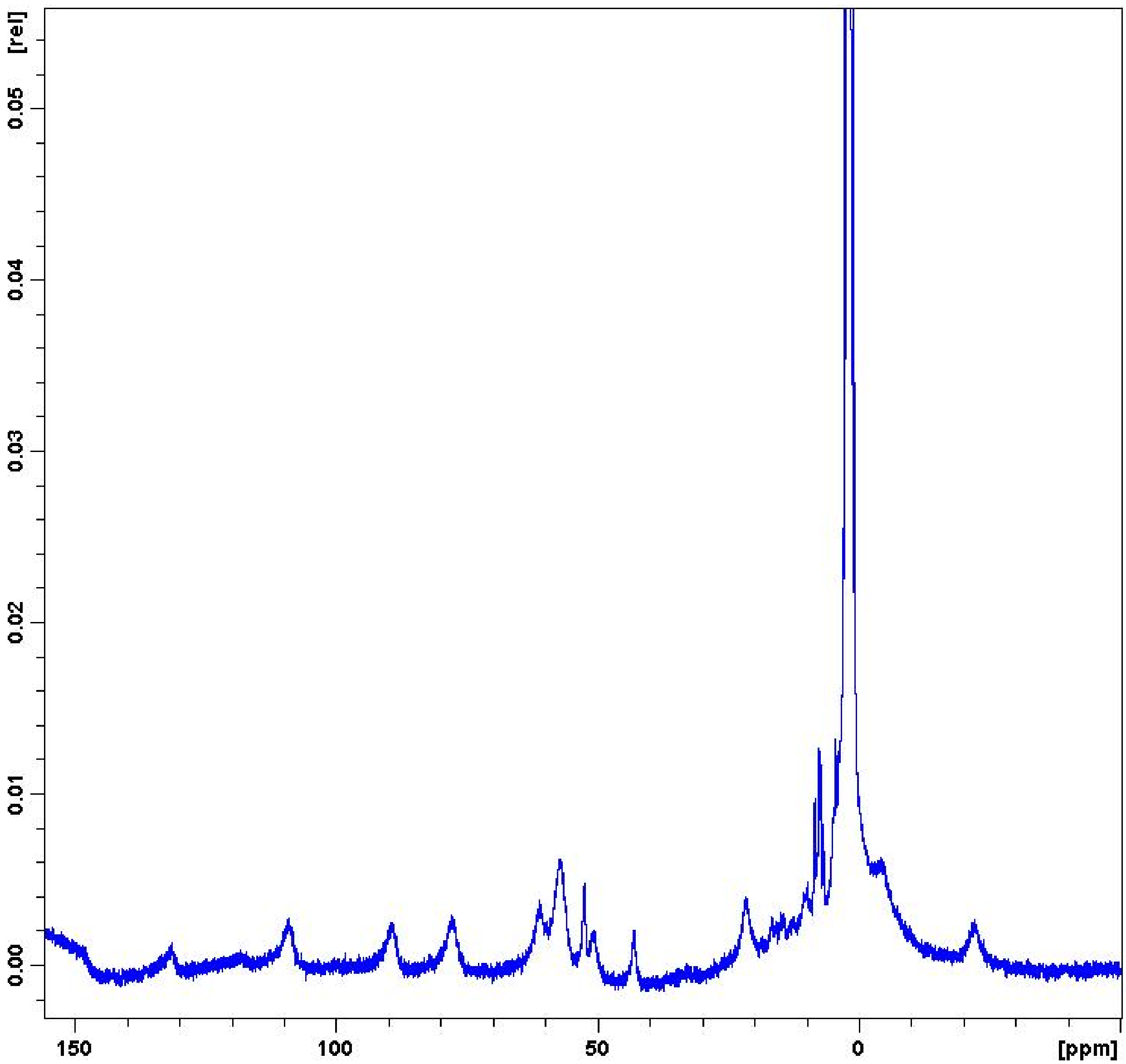

Figure S7. ^{1}H NMR spectrum of a 20 mM solution of [Fe(L^{Me}2)Cl$_2$] in CD$_3$CN. Major peaks outside the diamagnetic region: δ 131.4, 118.0, 109.2, 89.3, 77.9, 61.1, 57.2, 52.8, 50.7, 43.0, 21.7, 10.1, -4.4, -22.3. These data were recorded on a 250 MHz NMR instrument.

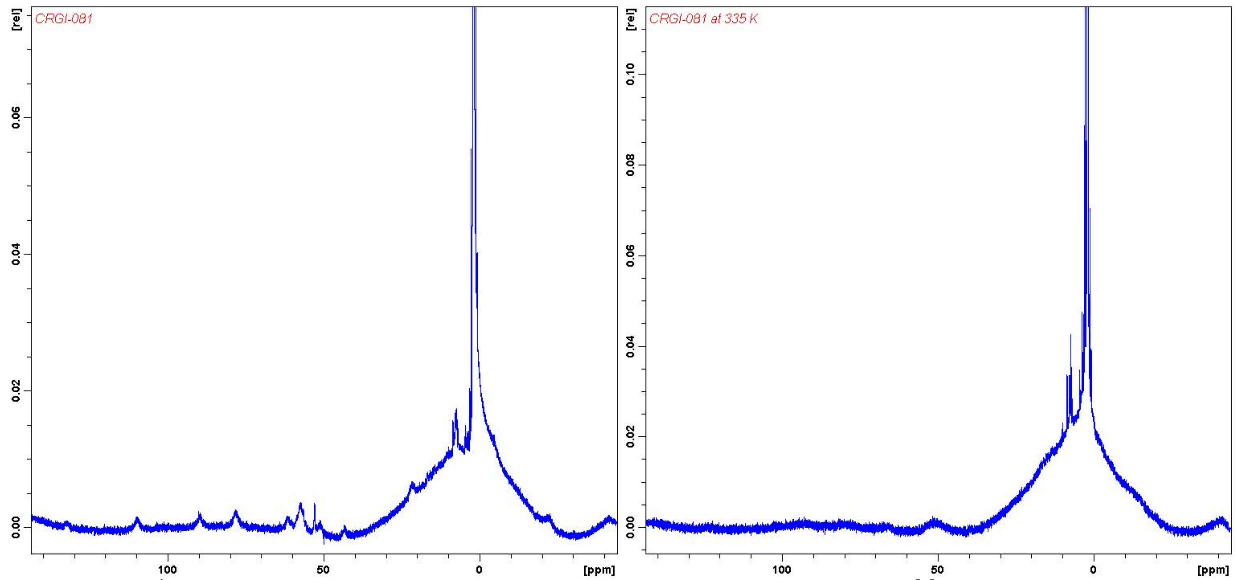

Figure S8. ^1H NMR spectra (400 MHz) of a 20 mM solution of $[Fe(L^{Me}2)Cl_2]$ in CD_3CN at 294 K (left) and 335 K (right).

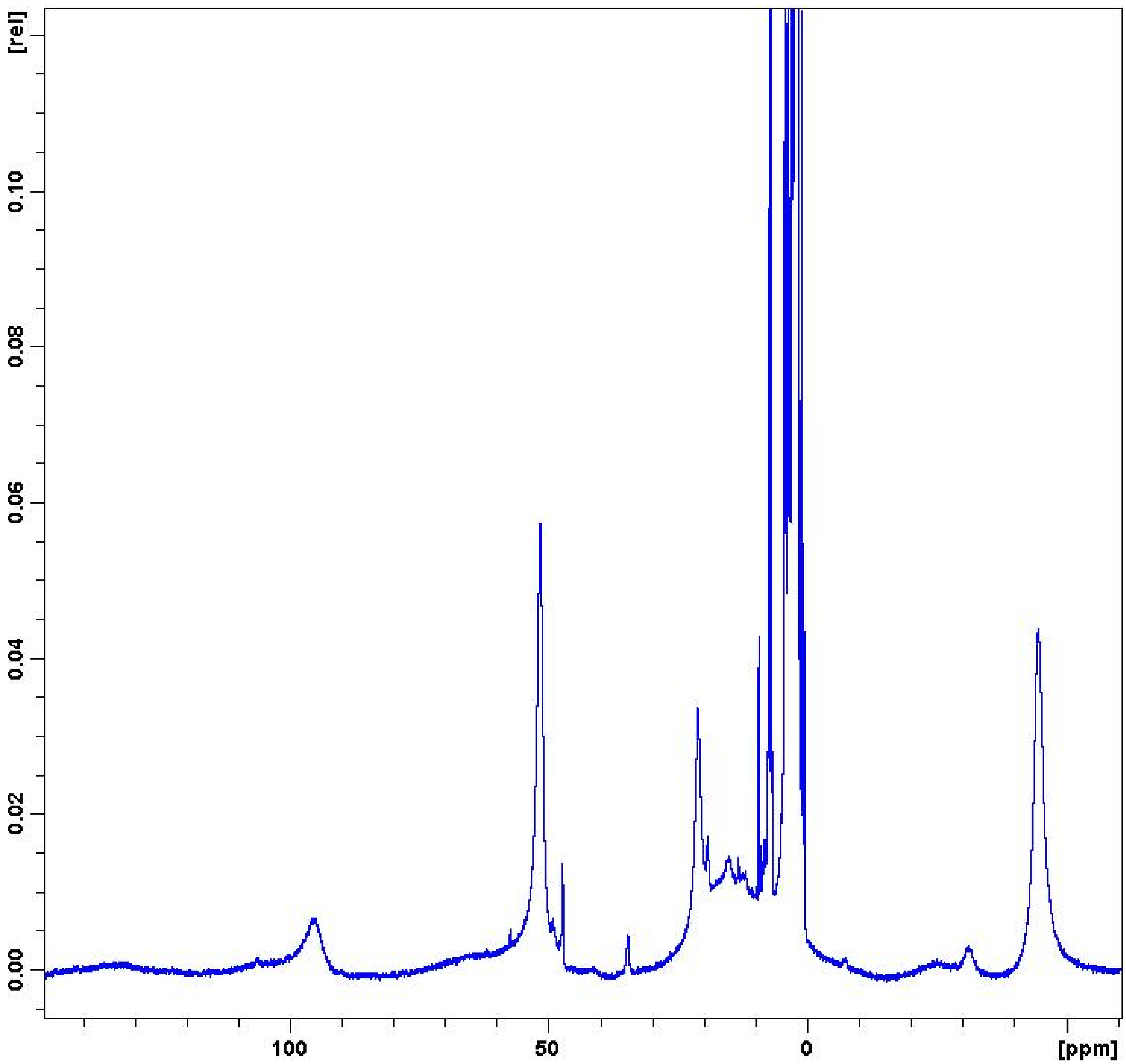

Figure S9. ^{1}H NMR spectrum of a 20 mM solution of [Fe(L^{Me}4)Cl_2] in CD_3CN. Major peaks outside the diamagnetic region: δ 133.9, 106.4, 65.0, 51.7, 47.4, 35.1, 21.5, 19.3, 14.8, -7.3, -31.1, -44.7. These data were recorded on a 250 MHz NMR instrument.

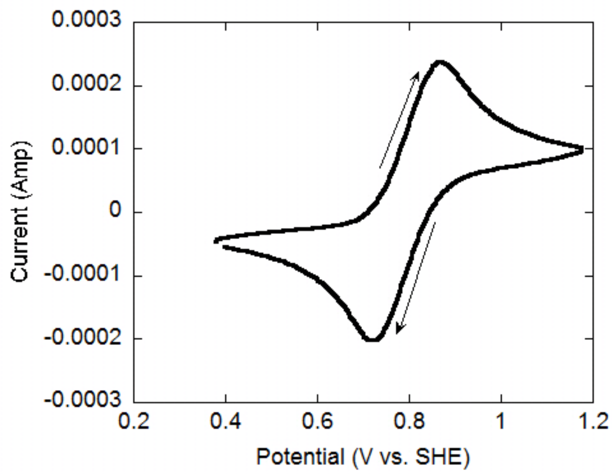

Figure S10. Cyclic voltammogram for $[Mn(L)Cl_2]$ in a 0.10 M solution of tetrabutylammonium perchlorate in acetonitrile. L = *N,N*-bis(2-pyridylmethyl)-1,2-ethanediamine. Ferrocene was subsequently added to reference the spectrum. For this particular scan: E_{pc} = 870 mV vs SHE, I_{pc} = 2.4 × 10^{-4} Amp, E_{pa} = 721 mV vs SHE, I_{pa} = 2.3 × 10^{-4} Amp, $E_{1/2}$ = +795 mV vs. SHE, ΔE = 149 mV. The arrows indicate the direction of the scan.

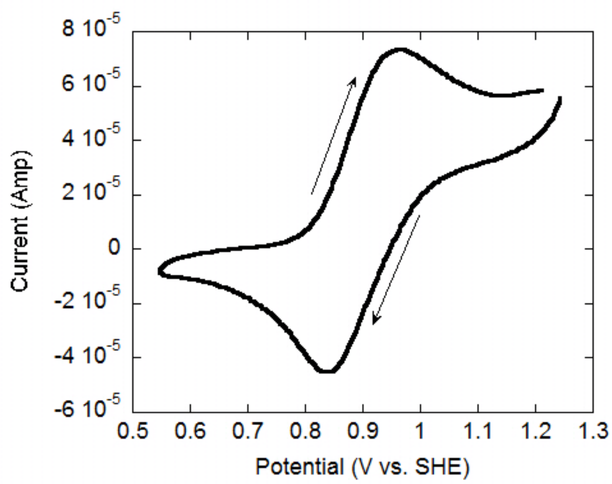

Figure S11. Cyclic voltammogram for $[Mn(L^{Me}1)Cl_2]$ in a 0.10 M solution of tetrabutylammonium perchlorate in acetonitrile. $L^{Me}1$ = *N*-methyl-*N,N'*-bis(2-pyridylmethyl)-1,2-ethanediamine. Ferrocene was subsequently added to reference the spectrum. For this particular scan: E_{pc} = 963 mV vs SHE, I_{pc} = 6.9 × 10^{-5} Amp, E_{pa} = 837 mV vs SHE, I_{pa} = 6.1 × 10^{-5} Amp, $E_{1/2}$ = +900 mV vs. SHE, ΔE = 126 mV. The arrows indicate the direction of the scan.

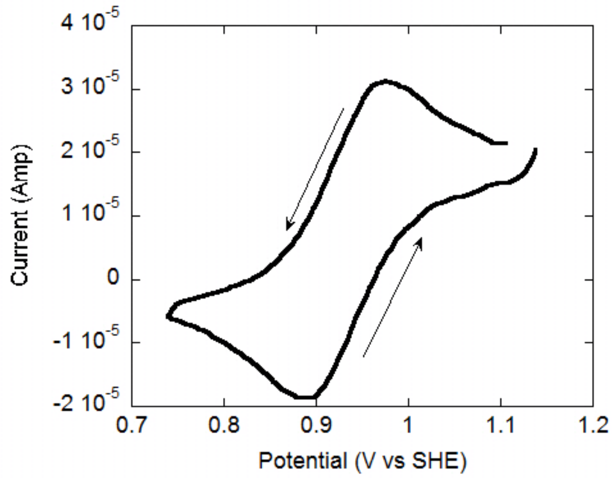

Figure S12. Cyclic voltammogram for $[Mn(L^{Me}2)Cl_2]$ in a 0.10 M solution of tetrabutylammonium perchlorate in acetonitrile. $L^{Me}2$ = *N,N'*-dimethyl-*N,N'*-bis(2-pyridylmethyl)-1,2-ethanediamine. Ferrocene was subsequently added to reference the redox features. For this particular scan: E_{pc} = 976 mV vs SHE, $I_{pc} = 2.6 \times 10^{-5}$ Amp, E_{pa} = 888 mV vs SHE, $I_{pa} = 2.5 \times 10^{-5}$ Amp, $E_{1/2}$ = +932 mV vs. SHE, ΔE = 88 mV. The arrows indicate the direction of the scan.

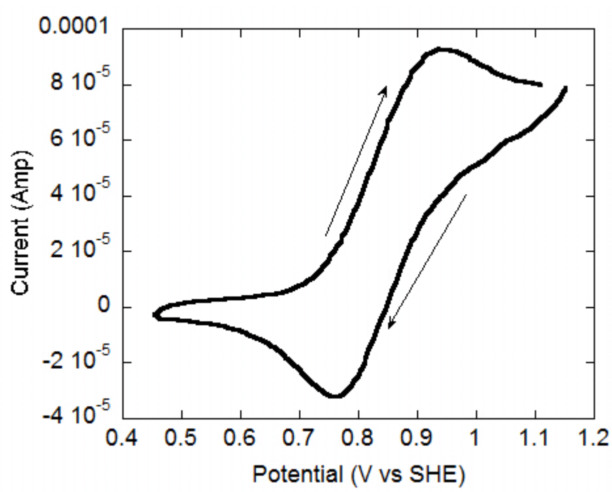

Figure S13. Cyclic voltammogram for $[Mn(L^{Me}2')Cl_2]$ in a 0.10 M solution of tetrabutylammonium perchlorate in acetonitrile. $L^{Me}2'$ = *N,N'*-bis(6-methyl-2-pyridylmethyl)-1,2-ethanediamine. Ferrocene was subsequently added to reference the redox features. For this particular scan: E_{pc} = 940 mV vs SHE, $I_{pc} = 8.6 \times 10^{-5}$ Amp, E_{pa} = 767 mV vs SHE, $I_{pa} = 5.0 \times 10^{-5}$ Amp, $E_{1/2}$ = +854 mV vs. SHE, ΔE = 173 mV. The arrows indicate the direction of the scan.

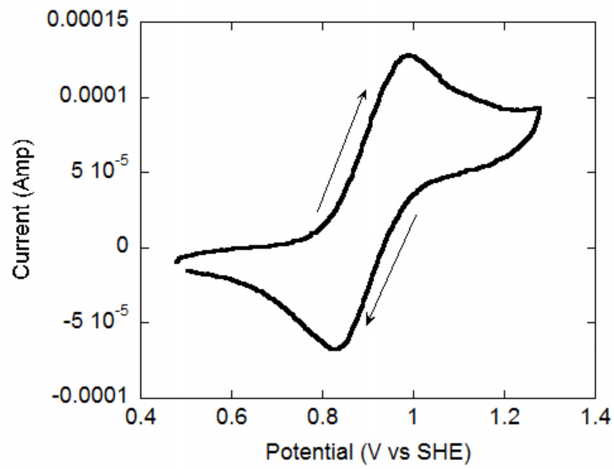

Figure S14. Cyclic voltammogram for $[Mn(L^{Me}3)Cl_2]$ in a 0.10 M solution of tetrabutylammonium perchlorate in acetonitrile. $L^{Me}3$ = *N*-methyl-*N,N'*-bis(6-methyl-2-pyridylmethyl)ethane-1,2-diamine. Ferrocene subsequently added as an internal reference. For this particular scan: E_{pc} = 987 mV vs SHE, $I_{pc} = 1.23 \times 10^{-4}$ Amp, E_{pa} = 829 mV vs SHE, $I_{pa} = 9.7 \times 10^{-5}$ Amp, $E_{1/2}$ = +908 mV vs. SHE, ΔE = 158 mV. The arrows indicate the direction of the scan.

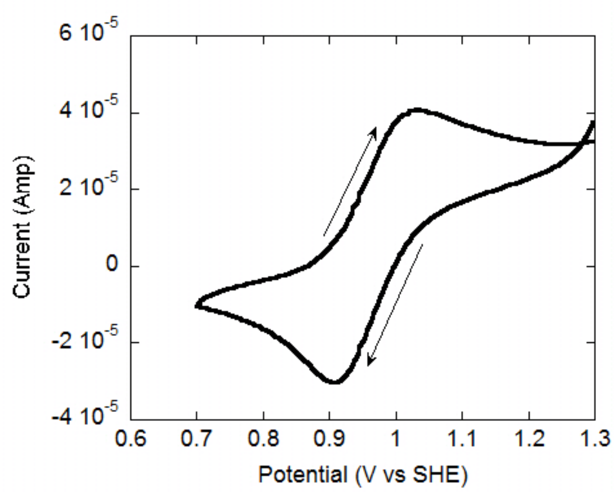

Figure S15. Cyclic voltammogram for $[Mn(L^{Me}4)Cl_2]$ in a 0.10 M solution of tetrabutylammonium perchlorate in acetonitrile. $L^{Me}4$ = *N,N*'-dimethyl-*N,N'*-bis(6-methyl-2-pyridylmethyl)-1,2-ethanediamine. Ferrocene was subsequently added to reference the redox features. For this particular spectrum: E_{pc} = 1034 mV vs SHE, $I_{pc} = 3.6 \times 10^{-5}$ Amp, E_{pa} = 907 mV vs SHE, $I_{pa} = 3.7 \times 10^{-5}$ Amp, $E_{1/2}$ = +971 mV vs. SHE, ΔE = 127 mV. The arrows indicate the direction of the scan.

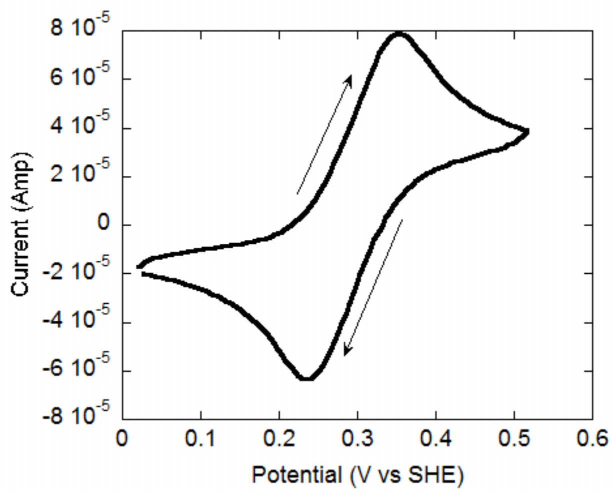

Figure S16. Cyclic voltammogram for $[Fe(L)Cl_2]$ in a 0.10 M solution of tetrabutylammonium perchlorate in acetonitrile. L = *N,N*-bis(2-pyridylmethyl)-1,2-ethanediamine. Ferrocene is subsequently added to reference the redox features. For this particular scan: E_{pc} = 349 mV vs SHE, $I_{pc} = 7.7 \times 10^{-5}$ Amp, E_{pa} = 228 mV vs SHE, $I_{pa} = 7.1 \times 10^{-5}$ Amp, $E_{1/2}$ = +289 mV vs. SHE, ΔE = 121 mV. The arrows indicate the direction of the scan.

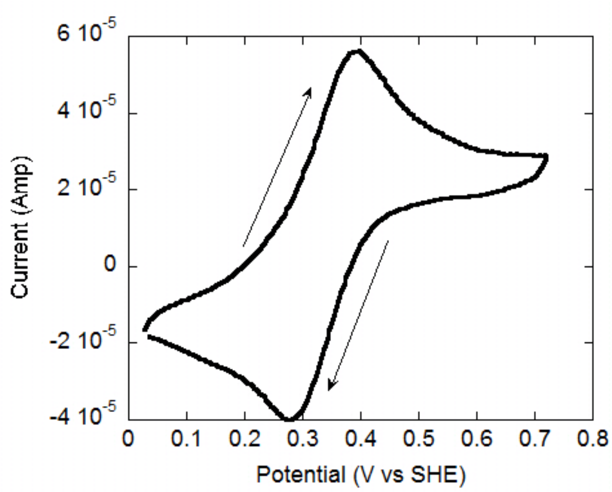

Figure S17. Cyclic voltammogram for $[Fe(L^{Me}1)Cl_2]$ in a 0.10 M solution of tetrabutylammonium perchlorate in acetonitrile. $L^{Me}1$ = *N*-methyl-*N,N'*-bis(2-pyridylmethyl)-1,2-ethanediamine. Ferrocene is subsequently added as an internal standard. For this particular scan: E_{pc} = 389 mV vs SHE, $I_{pc} = 4.8 \times 10^{-5}$ Amp, E_{pa} = 275 mV vs SHE, $I_{pa} = 5.1 \times 10^{-5}$ Amp, $E_{1/2}$ = +332 mV vs. SHE, ΔE = 114 mV. The arrows indicate the direction of the scan.

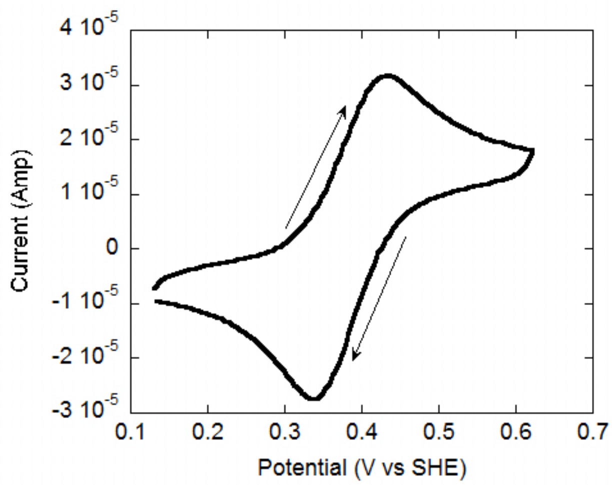

Figure S18. Cyclic voltammogram for [Fe($L^{Me}2$)Cl_2] in a 0.10 M solution of tetrabutylammonium perchlorate in acetonitrile. $L^{Me}2$ = *N,N'*-dimethyl-*N,N'*-bis(2-pyridylmethyl)-1,2-ethanediamine. Ferrocene is subsequently added as an internal standard. For this particular scan: E_{pc} = 431 mV vs SHE, I_{pc} = 2.9 × 10^{-5} Amp, E_{pa} = 338 mV vs SHE, I_{pa} = 3.5 × 10^{-5} Amp, $E_{1/2}$ = +385 mV vs. SHE, ΔE = 93 mV. The arrows indicate the direction of the scan.

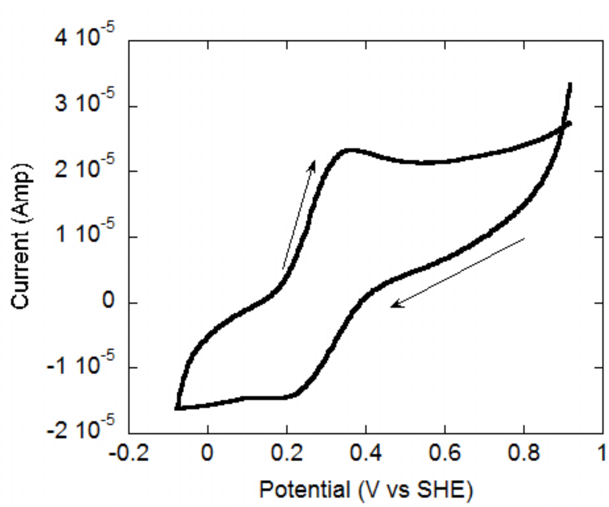

Figure S19. Cyclic voltammogram for [Fe($L^{Me}2'$)Cl_2] in a 0.10 M solution of tetrabutylammonium perchlorate in acetonitrile. $L^{Me}2'$ = *N,N*-bis(6-methyl-2-pyridylmethyl)-1,2-ethanediamine. Ferrocene was subsequently added to reference the redox features. For this particular scan: E_{pc} = 361 mV vs SHE, I_{pc} = 1.8 × 10^{-5} Amp, E_{pa} = 208 mV vs SHE, I_{pa} = 1.1 × 10^{-5} Amp, $E_{1/2}$ = +285 mV vs. SHE, ΔE = 153 mV. The arrows indicate the direction of the scan.

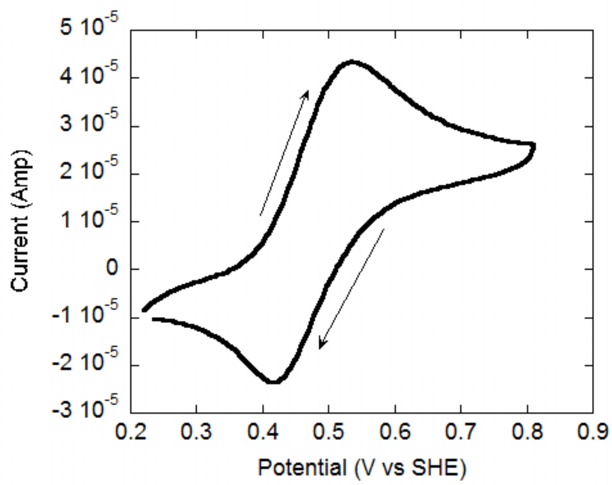

Figure S20. Cyclic voltammogram for $[Fe(L^{Me}3)Cl_2]$ in a 0.10 M solution of tetrabutylammonium perchlorate in acetonitrile. $L^{Me}3$ = *N*-methyl-*N,N'*-bis(6-methyl-2-pyridylmethyl)ethane-1,2-diamine. Ferrocene is subsequently added to reference the redox features. For this particular scan: E_{pc} = 534 mV vs SHE, $I_{pc} = 3.7 \times 10^{-5}$ Amp, E_{pa} = 418 mV vs SHE, $I_{pa} = 3.4 \times 10^{-5}$ Amp, $E_{1/2}$ = +476 mV vs. SHE, ΔE = 116 mV. The arrows indicate the direction of the scan.

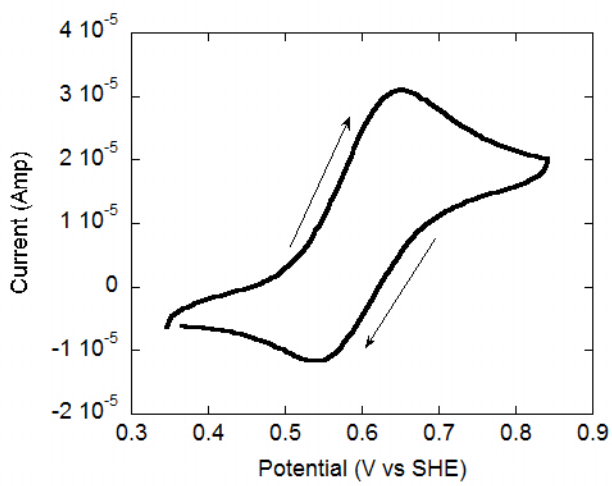

Figure S21. Cyclic voltammogram for $[Fe(L^{Me}4)Cl_2]$ in a 0.10 M solution of tetrabutylammonium perchlorate in acetonitrile. $L^{Me}4$ = *N,N*'-dimethyl-*N,N'*-bis(6-methyl-2-pyridylmethyl)-1,2-ethanediamine. Ferrocene is subsequently added as an internal standard. For this particular scan: E_{pc} = 651 mV vs SHE, $I_{pc} = 2.6 \times 10^{-5}$ Amp, E_{pa} = 541 mV vs SHE, $I_{pa} = 1.9 \times 10^{-5}$ Amp, $E_{1/2}$ = +596 mV vs. SHE, ΔE = 110 mV. The arrows indicate the direction of the scan.

Table S1. Selected crystallographic data for $[Mn(L)(H_2O)Cl]_2(MnCl_4)$, $[Mn(L^{Me}3)(H_2O)Cl_2]$, and $[Mn(L^{Me}2'\text{-ox})Cl_2]$.

Parameter	$[Mn(L)(H_2O)Cl]_2(MnCl_4)$	$[Mn(L^{Me}3)(H_2O)Cl_2$	$[Mn(L^{Me}2'\text{-ox})Cl_2]$
Formula	$C_{28}H_{40}Cl_6Mn_3N_8O_2$	$C_{17}H_{24}Cl_2MnN_4O$	$C_{16}H_{18}Cl_2MnN_4$
MW	898.2	426.24	392.18
cryst syst	Monoclinic	Monoclinic	Monoclinic
space group	*C2/c (#15)*	*$P2_1/c$ (#14)*	*C2/c (#15)*
a (Å)	28.4241(12)	11.3978(7)	12.0792(9)
b (Å)	8.5365(4)	8.7356(6)	9.6386(7)
c (Å)	19.0616(9)	20.5972(13)	15.2205(11)
α (deg)	90	90	90
β (deg)	122.7350(10)	104.7320(10)	101.7710(10)
γ (deg)	90	90	90
V ($Å^3$)	3890.6(3)	1983.4(2)	1734.8(2)
Z	4	4	4
Cryst color	Colorless	Colorless	Light amber
T (K)	193	193	193
Reflns collected	17021	19737	8565
Unique reflns	3922	3551	2150
R1 (F, I > 2σ(I))	0.0352	0.0543	0.0440
wR2 (F^2, all data)	0.0823	0.1417	0.1211

$R1 = \Sigma||F_o| - |F_c||/\Sigma||F_o|$; $wR2 = [\Sigma w(F_o^2-F_c^2)^2/\Sigma w(F_o^2)^2]^{1/2}$.

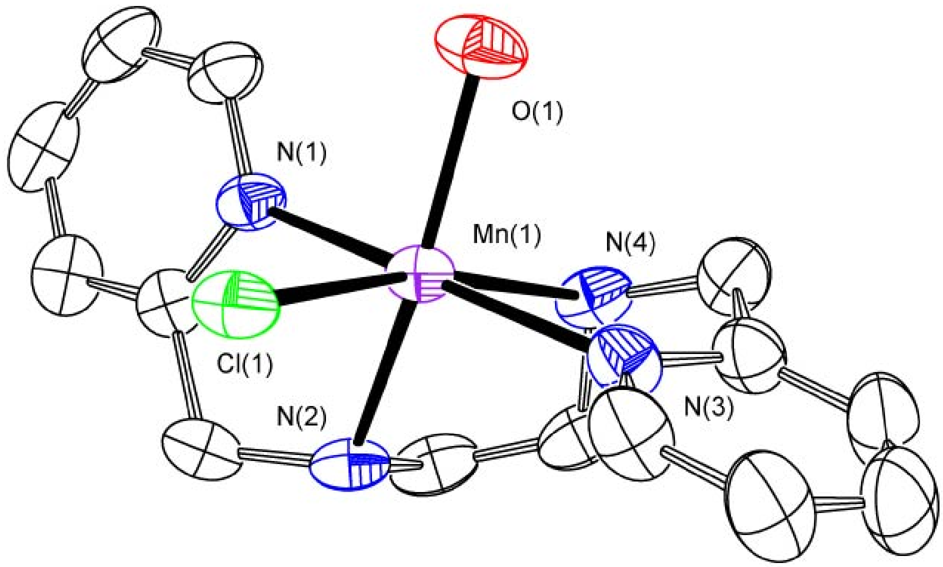

Figure S22. ORTEP representation of the crystal structure of the cation $[Mn(L)(H_2O)Cl]^+$. The hydrogen atoms and the other manganous species in the unit cell are omitted for clarity. Thermal ellipsoids are drawn at 50% probability.

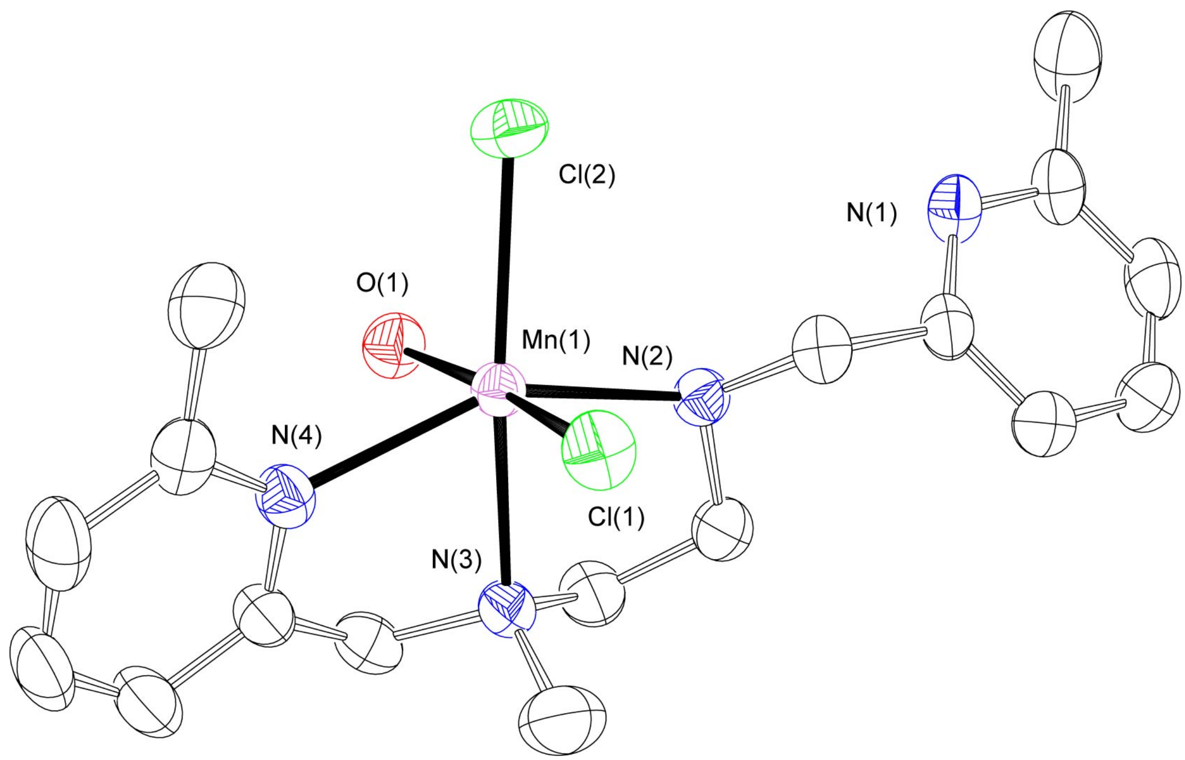

Figure S23. ORTEP representation of the crystal structure of $[Mn(L^{Me}3)(H_2O)Cl_2]$. Hydrogen atoms are omitted for clarity. Thermal ellipsoids are drawn at 50% probability.

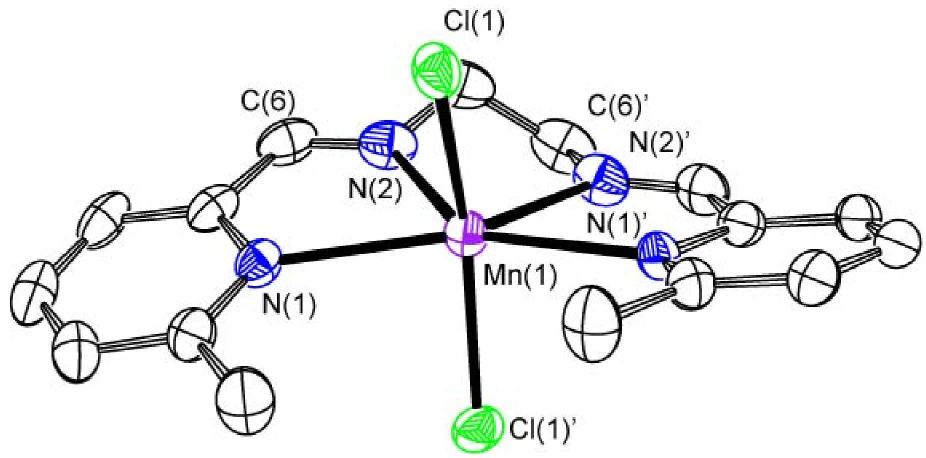

Figure S24. ORTEP representation of the crystal structure of [Mn(L^{Me}2'-ox)Cl_2]. Hydrogen atoms are omitted for clarity. Thermal ellipsoids are drawn at 50% probability. The N(2)-C(6) bonds have been oxidized to double bonds, as indicated by the N-C bond lengths, which contract from 1.46 to 1.25 angstroms. The Mn-N and Mn-Cl bond distances do not change significantly from those in [Mn(L^{Me}2')Cl_2]; these data and the pale color of the crystals suggest that the oxidation state of the manganese remains +2.